D. S. Bethune
J. R. Lankard
M. M. T. Loy
P. P. Sorokin

Time-Resolved Infrared Spectral Photography: A New Technique

A new technique for photographic or multichannel photoelectric recording of broad band infrared absorption spectra with approximately 5-ns time resolution is described. The technique is based on resonant four-wave mixing in alkali metal vapors.

A. Introduction

The ability to record a transient broad band infrared absorption spectrum has great applicability in studies of pulsed chemical reactions, such as those induced by flash photolysis or laser irradiation. Efforts to develop this capability have led to the demonstration of several techniques. One recent approach uses a pyroelectric vidicon tube in conjunction with an optical multichannel analyzer (OMA) [1]. Another approach utilizes an infrared upconversion technique [2] whereby infrared radiation is mixed with laser light in a nonlinear crystal to produce radiation at the sum frequency that can then be photographed. Still another approach, applicable only to repetitive events, is based on Fourier transform spectroscopy [3].

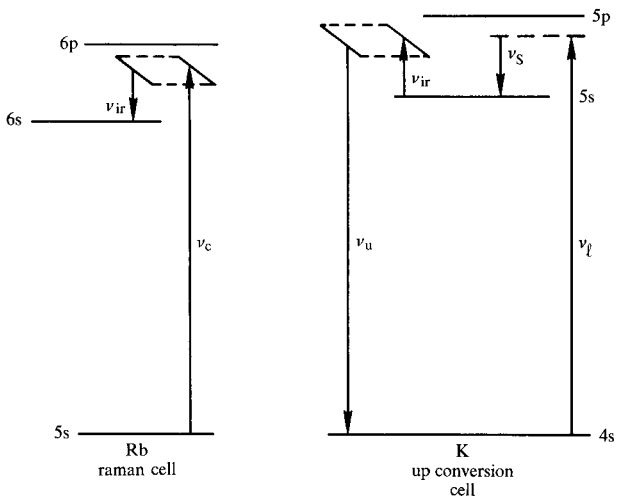

Figure 1 Level diagrams for the Raman generation and four-wave upconversion processes; ν_c and ν_{ir}—broad band visible and ir continua; ν_ℓ and ν_s—narrow band visible laser and its Stokes beam; ν_u—upconverted visible beam.

We recently introduced a new technique for single-shot recording of broad band infrared absorption spectra [4]. Our method is similar to that described in Ref. [2] in that it uses nonlinear optics for infrared upconversion. However, unlike the case of Ref. [2], in which quadratic nonlinearities of noncentrosymmetric crystals are utilized, we use resonantly enhanced third-order optical nonlinearities of metal vapors [5], both to produce a pulsed ir continuum that probes the sample and to upconvert this ir continuum into the visible. These two processes are diagrammed in Fig. 1. Our method, which has a time resolution of 5 ns, provides a new approach to the problem of recording transient broad band ir spectra.

This paper describes the present state of development of our technique of broad band infrared spectral photography. The technique has the potential for probing much of the 2- to 20-μm spectral region, the so-called "finger-

Table 1 Alkali resonance lines and corresponding $np \rightarrow ns$ infrared frequencies.

Alkali	*Resonance lines*		*Infrared transitions*		
	Transition	*Wavelength* (nm)	*Transition*	*Frequency* (cm^{-1})	*Wavelength* (μm)
Cs	$6s \rightarrow 7p_{3/2}$	455.7	$7p_{3/2} \rightarrow 7s$	3411	2.93
	$6s \rightarrow 7p_{1/2}$	459.4	$7p_{1/2} \rightarrow 7s$	3230	3.10
	$6s \rightarrow 8p_{3/2}$	387.7	$8p_{3/2} \rightarrow 8s$	1475	6.78
	$6s \rightarrow 8p_{1/2}$	389.0	$8p_{1/2} \rightarrow 8s$	1392	7.18
	$6s \rightarrow 9p_{3/2}$	361.2	$9p_{3/2} \rightarrow 9s$	771	12.96
	$6s \rightarrow 9p_{1/2}$	361.8	$9p_{1/2} \rightarrow 9s$	727	13.76
	$6s \rightarrow 10p_{3/2}$	347.8	$10p_{3/2} \rightarrow 10s$	454	22.04
	$6s \rightarrow 11p_{3/2}$	339.9	$11p_{3/2} \rightarrow 11s$	291	34.35
Rb	$5s \rightarrow 6p_{3/2}$	420.3	$6p_{3/2} \rightarrow 6s$	3659	2.73
	$5s \rightarrow 6p_{1/2}$	421.7	$6p_{1/2} \rightarrow 6s$	3582	2.79
	$5s \rightarrow 7p_{3/2}$	358.8	$7p_{3/2} \rightarrow 7s$	1559	6.42
	$5s \rightarrow 8p_{3/2}$	335.0	$8p_{3/2} \rightarrow 8s$	807	12.39
K	$4s \rightarrow 5p_{3/2}$	404.5	$5p_{3/2} \rightarrow 5s$	3693	2.71
	$4s \rightarrow 5p_{1/2}$	404.8	$5p_{1/2} \rightarrow 5s$	3674	2.72

print'' region of organic molecules. The basis for this contention is as follows. If a sufficiently intense broad band visible or uv continuum beam ν_c is applied to an alkali metal vapor in the region of any resonance line indicated in Table 1, stimulated electronic Raman scattering (SERS) results, producing a broad band ir Raman Stokes continuum ν_{ir} in the region of the corresponding infrared $np \rightarrow ns$ transition [4]. The ir continuum tends to have the same spectral bandwidth as the visible/uv pump continuum, and its spectral center of gravity shifts by the same amount (in cm^{-1}) as that of the pump continuum when the latter is shifted away from the np resonance lines. However, since SERS thresholds increase fairly rapidly as pump continua are shifted away from resonance lines, it has not been determined how far this procedure may be extended.

By application of pump continua centered at $\approx$405 nm in potassium vapor and $\approx$420 nm in rubidium vapor, we were able initially to cover the range $\approx$3500 to 4000 cm^{-1} [4]. We have since redesigned the experimental apparatus to produce a more intense visible/uv continuum beam. Working with the basic $6p \rightarrow 6s$ Raman Stokes transition in Rb ($\approx$3600 cm^{-1}), we are now able to cover continuously the ir range from $\approx$2600 to 4000 cm^{-1}, which includes the important CH vibrational stretch region. Because we use the third harmonic of a Nd^{3+}:YAG laser (λ = 0.355 μm) to pump the dye continua in our apparatus, we are presently limited to studying ir regions that can be reached with Stokes radiation based on the following alkali transitions: Cs: $7p \rightarrow 7s$, $8p \rightarrow 8s$; Rb: $6p \rightarrow 6s$; K: $5p \rightarrow 5s$. Two as yet untested modifications suggested later (Section E) may enable other ir regions to be probed using the same Nd^{3+}:YAG driver. Aside from this, it would appear that longer-wavelength ir regions can be reached in a straightforward manner with the use of the recently developed XeCl excimer laser (λ = 0.308 μm) to excite dye continua.

In Section B details of the experimental apparatus are given; we hope to encourage others to use and perhaps improve this technique. In Section C we first present and discuss static ir absorption spectra obtained by this technique. These spectra reveal some unusual aspects of the various mechanisms operative in both the Raman generation and upconversion processes, which the theory in Section D later addresses. To illustrate that the method can be used to record transient spectra, we also present recently obtained spectral photographs of the laser-induced isomerization of methyl isocyanide in Section C.

An assessment is made of the overall strengths and weaknesses of the method in Section E. At present, the most important defect appears to be the occurrence of a persistent random spectral noise, whose origins we have been unable to trace. As seen in many of the displayed spectra, this noise seriously detracts from the quality of the single-shot spectral photographs.

B. Experimental technique

Our technique for ir spectral photography uses resonant third-order nonlinearities of alkali metal vapor in two complementary processes (see Fig. 1). In the first process, SERS produces a broad band ir continuum from a broad band visible continuum. In the second process, which occurs after the ir continuum beam has probed the

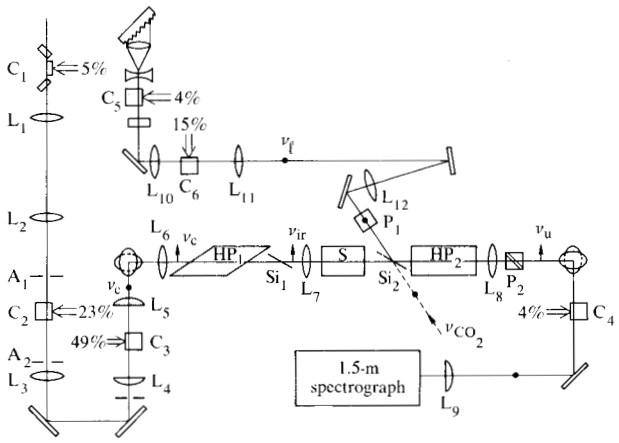

Figure 2 Diagram of experimental apparatus.

sample, resonant four-wave mixing upconverts the ir spectrum back into the visible, where it can be recorded photographically or photoelectrically.

These steps are accomplished with the apparatus shown in Fig. 2. The pump radiation for all six transversely pumped dye cells is the third harmonic beam ($\lambda = 0.355\ \mu$m) generated from a Quanta-Ray (Mountain View, CA 94043) Nd^{3+}:YAG oscillator-amplifier combination. The vertically polarized uv pump beam was expanded to a diameter of approximately 12 mm and subsequently apportioned into various channels by means of coated beam splitters. Each portion was ultimately focused with a cylindrical lens onto a dye cell through an NaCl diffuser made by wetting one surface of an NaCl window and allowing it to dry. The purpose of this intentional blurring of the pump beam was to produce a relatively uniform rectangular pumped region in each dye cell.

The visible continuum was produced by a three-stage system. The first cell C_1, which produced a superfluorescent beam $\approx 1000\ cm^{-1}$ wide, had windows tilted at approximately 10° to eliminate reflection feedback. Three lenses (L_1, L_2, L_3), a pair of apertures (A_1, A_2), and a preamplifier cell (C_2) were used to produce a well-collimated amplified beam, which was then sent to the final amplifier C_3. Care was taken to keep the (C_1, C_2) and (C_2, C_3) cell separations large enough to prevent interactive feedback between the various cells. To avoid very high pump intensities at cell C_3, the continuum beam was compressed horizontally but not vertically. Cylindrical lenses L_4 and L_5 were used for this purpose.

The uv pumping beam and the dye laser beams passing through the various dye cells were all vertically polarized. Two mirrors tilted at 45° to the horizontal, with centers vertically aligned, were used to rotate the plane of polarization of the continuum beam from the vertical to the horizontal in the section of the optical path occupied by the two heat-pipe ovens. Lens L_6 was a 50-cm lens that focused the visible continuum beam into the center of the Raman cell HP_1. For most of the studies reported here, HP_1 was a Rb-vapor heat-pipe oven operating at ≈ 1 kPa (9 torr). Both ends of HP_1 were terminated in Brewster angle windows, the output window being of LiF or BaF_2 to pass the broad band ir beam ν_{ir} generated in HP_1. The input window of HP_2 was also made of BaF_2, as was the 30-cm lens L_7 that focused the ir beam into the center of HP_2. The 18-cm gaseous sample cell was equipped with NaCl windows.

The tunable narrow band dye laser beam ν_ℓ, generated in a standard Hänsch-type configuration incorporating cell C_5 and subsequently amplified in cell C_6, was predominantly vertically polarized. A Glan prism P_1 rejected any remnant horizontally polarized component of ν_ℓ. A 100-cm lens L_{12} brought beam ν_ℓ to a focus at the center of the upconverter heat-pipe HP_2. In all this work we have used K vapor at ≈ 0.6 kPa (5 torr) in HP_2. The portion of ν_ℓ transmitted through HP_2 could be almost completely nulled by the Glan prism P_2 without attenuation of the upconverted beam ν_u, since the latter is generated with horizontal polarization.

Two polished silicon wafers (Si_1, Si_2), set at Brewster's angle for the infrared, served multiple functions. The visible continuum ν_c was blocked by Si_1; Si_2 coupled the beam ν_ℓ into the second heat-pipe oven and coupled the CO_2 laser beam into the sample cell when needed to initiate reactions to be monitored by spectral photography. These silicon wafers afford broad band ir capabilities not provided by the Glan prism originally used [4] to combine the beams.

The upconverted beam ν_u, collimated by lens L_8 and with its polarization rotated back to vertical, was then sent to an optional amplifier dye cell C_4 and finally, for recording, to a 1.5-m grating spectrograph with entrance slits generally set at 50 μm. A cylindrical lens L_9 focused the beam on the slit. All optical paths were adjusted for proper timing of the visible continuum and dye laser pulses with respect to the 5-ns uv pump pulse. The pulses ν_ℓ and ν_c (ν_{ir}) were also arranged to be synchronous at the position of the beam-combining element Si_2.

Continuum and dye laser powers were measured with a Scientech power meter (Scientech, Inc., Boulder, CO 80303) with the system operating at 10 pulses per second (pps). Typically, at the entrance to HP_1, the 2-mm-diame-

ter continuum beam ν_c was measured to have ≈3–5 mJ of energy per pulse. The highest pulse energy we have measured for ν_c was 10 mJ, with p-bis(o-methylstyryl)benzene (bis-MSB) in p-dioxane used in cells C_1 and C_2 and p-bis[2-(5-phenyloxazolyl)benzene] (POPOP) in p-dioxane used in cell C_3. The maximum energy per pulse produced at 0.355 μm by the Quanta-Ray laser is ≈100 mJ. For the beam ν_ℓ, the energy per pulse measured just after the amplifier cell C_6 was usually ≈1 mJ. Diphenyl stilbene (DPS) in p-dioxane was used in cells C_5 and C_6 in all of these experiments. Dye cells C_2, C_4, C_5, and C_6 were fused quartz cells, 1 cm on a side, tilted at Brewster's angle for maximum transmission of the vertically polarized dye laser beams. They were equipped with small magnetically driven stirrers, as was cell C_1. In the case of cell C_3, the dye solution continuously circulated from a one-liter reservoir. As a general rule, dye solutions were changed at least once a day in the smaller cells.

The procedure for alignment is relatively straightforward and simply involves overlapping ν_ℓ and ν_c coaxially in HP_2. Convenient indicators that the Raman thresholds are exceeded are a narrow band yellow beam [5] ($\nu_\ell - 2\nu_S$) produced in the second cell and its broad band analogue, an orange continuum beam ($\nu_c - 2\nu_{ir}$) produced in the first cell. Since these beams propagate coaxially with ν_ℓ and ν_c, respectively, they can also be used for alignment purposes.

With the ir continuum blocked, the narrow band laser beam ν_ℓ is nulled by adjusting P_2. Unblocking ν_{ir} then makes visible the upconverted beam, which is well collimated and generally bright enough to be easily seen in a dimly lit room. Cell C_4 is used to amplify the weaker portions of the upconverted beam spectrum. These usually correspond to the limits of the ir probing range.

C. Experimental results

Discussion of the photographically recorded spectra can be conveniently divided into three parts. We first present and discuss ir spectra obtained when the pump continua are approximately centered on the K 5p or Rb 6p resonance lines, as in Ref. [4]. As Table 1 shows, the 2.7-μm region is probed in both cases. Water vapor bands and combination bands of CO_2 fall naturally in this range. In the second part, we discuss spectra obtained more recently. Here a serious effort has been made to shift the ir region to longer wavelengths, as far as possible from 2.7 μm. Rubidium was used exclusively in the Raman cell in this phase of our work. We have been able to extend the ir range out to the CH stretching region (≈3.2–3.6 μm). In the third part we demonstrate that the system is, indeed, capable of recording transient nonrepetitive ir absorption spectra. The example we have chosen is the laser-induced isomerization of methyl isocyanide (CH_3NC) to methyl cyanide (CH_3CN).

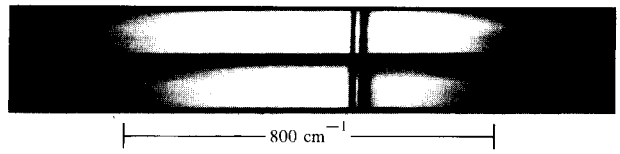

Figure 3 Diphenyl stilbene (DPS) continuum spectrum (first order) photographed through ≈0.7 kPa (5 torr) K vapor; two exposures shown. The absorption lines are the K 4s → 5p doublet.

• *The 2.7-μm region: CO_2 and H_2O bands*

Figure 3 shows the ν_c continuum spectrum obtained with the dye DPS in p-dioxane, photographed through ≈0.6 kPa (5 torr) of potassium vapor, with the grating spectrograph used in first order. This spectrum was obtained with the apparatus of Ref. [4]. In this case, a spectral band ≈800 cm^{-1} wide that encompasses the two K resonance lines at 404.5 and 404.8 nm is observed. The corresponding upconverted spectrum, with K vapor in HP_2, is shown in Fig. 4(a). A relatively smooth spectrum ≈400 cm^{-1} wide is observed. Two strong dark lines correspond to absorption at the K 4s → $5p_{1/2,3/2}$ frequencies. Between these, roughly twice as close to the 4s → $5p_{1/2}$ line as to the 4s → $5p_{3/2}$ line, there occurs a sharp dark line which we attribute to a cancellation of the $5p_{1/2}$ and $5p_{3/2}$ contributions to the Raman susceptibility. The upconverted output is rigorously proportional to $|\chi^{(3)}_{xxyy}|^2$; for s → p → s Raman transitions, $\chi^{(3)}_{xxyy} = \chi^{(3)}_{xxxx}$, the symmetric part of the Raman tensor. The observed cancellation in the symmetric term of the Raman susceptibility is a predicted feature for all alkali metal atoms [5, 6].

The spectra shown in Figs. 4(b) and (c) were photographed with increasing amounts of CO_2 gas admitted to the 18-cm-long sample cell, which was evacuated in the case of Fig. 4(a). Two well-known CO_2 band systems are observed, the 02^01 band at 3609 cm^{-1} and the stronger 10^01 system, with band head at 3716 cm^{-1}. In both cases the P and R branches are clearly evident. The overexposed line obscuring part of the R branch of the 3609-cm^{-1} system is incompletely nulled light from the arbitrarily tuned laser at ν_ℓ.

The bright doublet on the left-hand side of each spectrum represents upconversion of lasing on the K ir transition $5p_{3/2,1/2}$ → 3d. As in previous studies made with narrow band laser excitation [5], lasing on these transitions evidently occurs in the second cell, and perhaps also in the first, together with the broad band Raman radiation when the DPS continuum is applied. The role of these

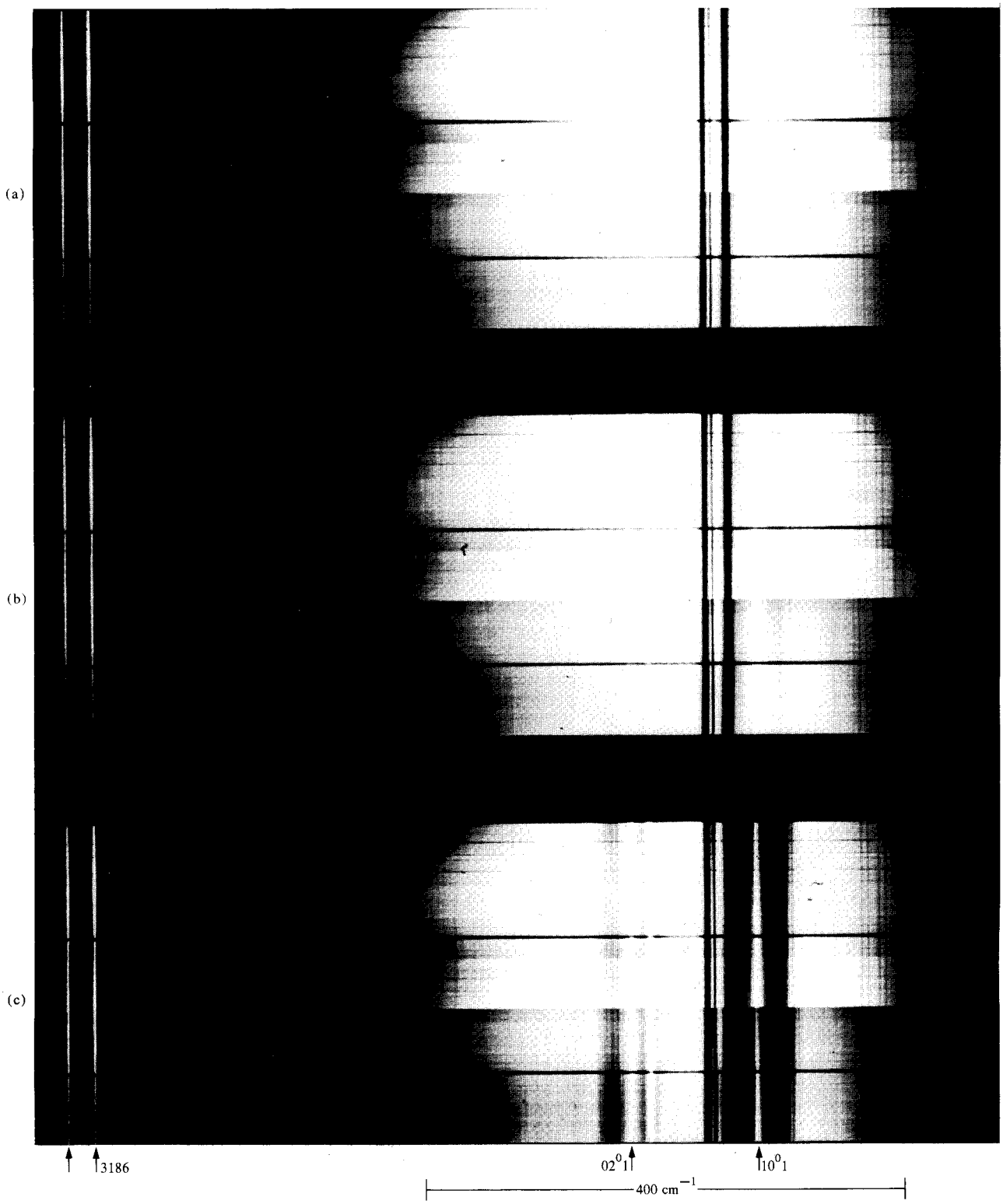

Figure 4 Upconverted DPS K-K spectrum (first order) with sample cell (a) evacuated, (b) containing a small unmeasured amount of CO_2, and (c) containing ≈67 kPa (500 torr) CO_2. In all three cases two exposures are shown.

lasing lines is quite incidental to the ir photography process, but they do provide convenient frequency markers. The ir frequencies are 3165 and 3186 cm^{-1}; those corresponding to the K 5p-5s doublet are 3675 and 3693 cm^{-1}.

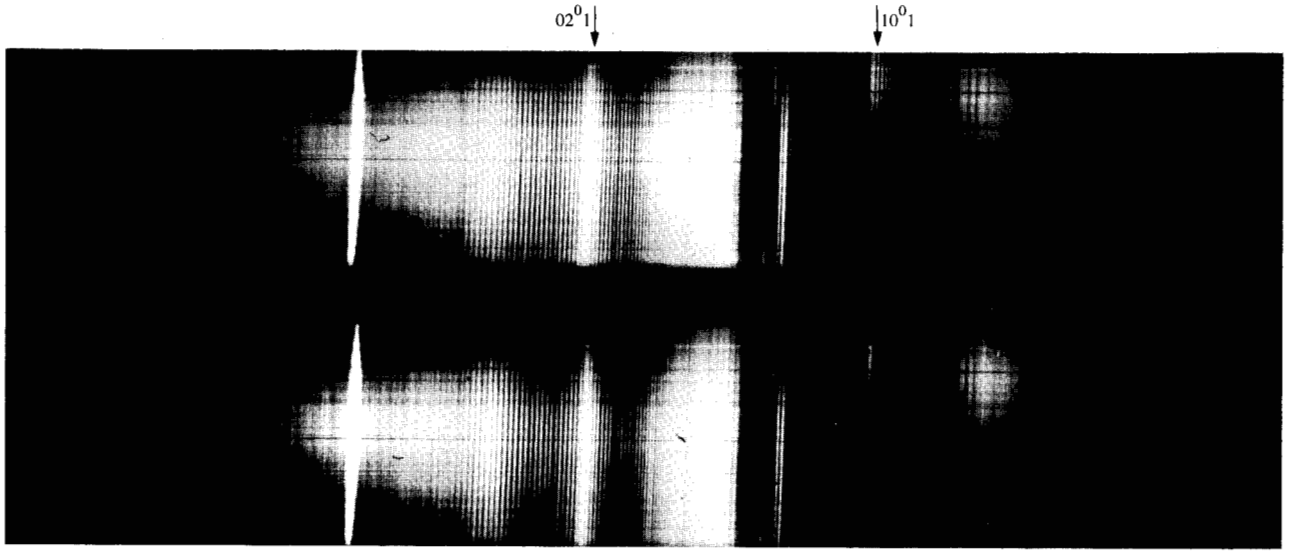

Figure 5 Upconverted DPS K-K spectrum (second order) containing increasing amounts (top to bottom) of CO_2 in the sample cell.

Each of these spectra represents many superimposed shots. Two exposures are shown for each pressure of gas in the sample cell.

With the spectrograph used in second order to obtain higher resolution, the rotational lines of the P and R branches of the CO_2 combination bands are clearly resolved, as shown in Fig. 5. At the peak of the P branch of the 3609-cm^{-1} band, adjacent CO_2 lines are known to be spaced ≈ 1.7 cm^{-1} apart. The observed ir resolution is ≈ 0.5 cm^{-1}, consistent with the resolution of our spectrograph and the ≈ 0.5-cm^{-1} linewidth of the tunable laser. Note that ν_ℓ has here been tuned completely off the 3609-cm^{-1} band. Tuning of ν_ℓ over a wide range does not greatly influence the appearance of the upconverted spectra.

For the upconverted spectrum of Fig. 6, a 0.6-kPa (5-torr) Rb cell and POPOP in p-dioxane were used to generate the ir continuum, and the sample cell was completely removed. The upconverter K cell and the narrow band DPS laser at ν_ℓ were unchanged. The wavelengths of the Rb $6p_{3/2,1/2} \rightarrow 6s$ transitions are quite close to those of the K $5p_{3/2,1/2} \rightarrow 5s$ transitions, so that similar regions in the ir are probed in Figs. 5 and 6. In Fig. 6 dark bands correspond to $4s \rightarrow 5p_{3/2,1/2}$ resonance absorptions of K atoms in the second cell and to absence of ir light at the exact $6p_{3/2,1/2} \rightarrow 6s$ frequencies of Rb. Between each of these absorption line pairs is a dark line due to interference nulls in $\chi^{(3)}_{xxyy}$ for K in the upconverter cell and in $\chi^{(3)}_{xxxx}$ for Rb in the Raman cell.

The myriad of sharp, dark lines on the high-frequency side of the spectrum in Fig. 6 results from residual water vapor in the optical path between the two vapor cells. A densitometer trace of a portion of the spectrum in Fig. 6 is shown in the upper portion of Fig. 7. The correspondence with a published IUPAC water vapor spectrum [7] (lower trace) is apparent. Water vapor lines may also be discerned in Fig. 4.

The spectra shown in this section were all taken under time-averaged conditions with the lower-power apparatus of Ref. [4]. Cell C_4 was not used for any of these spectra. More averaging was done for second-order spectra because of a fall-off in reflectivity of the spectrograph grating. One result of this averaging is that the random spectral noise mentioned previously is effectively averaged out, leaving well-resolved ir absorption bands with apparently correct intensity distributions.

• *The 2600–3600-cm^{-1} region: NH_3 and CH stretching vibrations*

Figure 8 shows a series of upconverted spectra taken on a dry day with no sample cell in place. Here, the frequency of the narrow band DPS laser ν_ℓ is successively stepped to shorter wavelengths as one proceeds along the sequence from top to bottom. Rubidium vapor was used in the Raman cell, and all three dye cells involved in the generation of the continuum beam were filled with a 7.5×10^{-4} molar solution of Stilbene 420 dye (Exciton, Dayton, OH 45431) in 1:1 H_2O-CH_3OH. Each spectrum represents four superimposed shots. Again, the upconverted beam was not amplified.

In this sequence the narrow band laser line is seen at the right, crossing first the band corresponding to the longer-wavelength Rb resonance line and then the null in

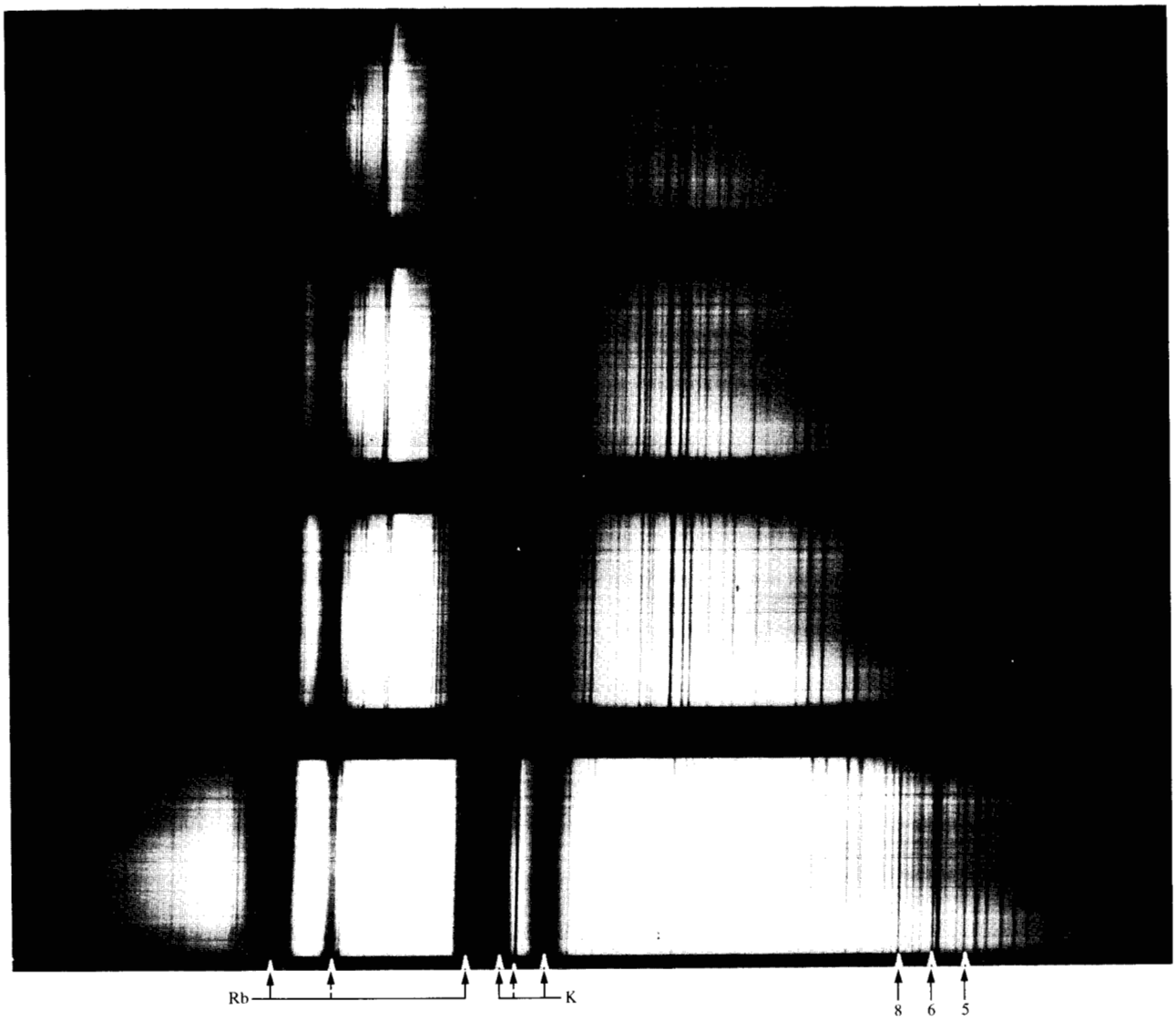

Figure 6 Upconverted POPOP Rb-K spectrum (second order, sample cell removed); increasing exposures (top to bottom). The numbers 8, 6, 5 refer to numbered peaks in the IUPAC calibration spectrum given in Fig. 7.

the Rb Raman susceptibility at 3607 cm^{-1}. The bright line that tunes at the left results entirely from processes occurring in the upconverter cell. The narrow band laser beam ν_ℓ evidently induces SERS on *both* transitions 4s → 5p → 5s and 4s → 5p → 3d in K cell HP_2. The narrow band Stokes beam produced by the latter process is then upconverted by four-wave mixing associated with the former process.

Figure 8 again demonstrates the relative unimportance of exact phase matching in the upconversion process. It also shows the random, granular appearance of the upconverted light when a limited number of shots are used.

Figure 9 shows a sequence of spectra taken under the same general conditions as in Fig. 8, except that the number of shots accumulated per exposure is varied. It is seen that at least ten shots (fifth spectrum) are necessary for good ir coverage out to ≈3000 cm^{-1}, the approximate position of the 4s → 5p → 3d Stokes line, seen upconverted at the left. Since this amount of light overexposes the spectrum corresponding to shorter ir wavelengths, we were eventually led to the use of an upconverted beam amplifier dye cell C_4, with its dye chosen to bias amplification towards longer visible (hence, also ir) wavelengths. The bottom few spectra of Fig. 9 contain particularly good representations of the positions of the Rb and

K resonance lines and their corresponding Raman nulls. The top spectra display the granular spectral character of the upconverted light. The dark line appearing on the high-frequency side of the upconverted K 5p-3d doublet appears in virtually all spectra covering this region. Its frequency ($\approx$3208 cm^{-1}) coincides with the K 4d-5f transitions. Potassium atoms in the 4d states are probably produced by photodissociation of K_2 dimers as the beam ν_ℓ passes through HP_2.

In Fig. 10 the wide range of ir covered with the use of dimethyl POPOP in cells C_1, C_2, and C_3 is demonstrated. The three lines at the left are upconversions of lasing transitions in the K cell HP_2. The brightest of these three lines is at 2730.5 cm^{-1} ($6s_{1/2} \rightarrow 5p_{3/2}$). A spectral region $\approx$1000 cm^{-1} in width can be spanned with a single continuum dye solution, provided several shots/plate exposure are allowed. Because of insufficient exposure, the single-shot spectrum covers only approximately 600 cm^{-1}.

In Fig. 11, 27 kPa (200 torr) of ammonia (NH_3) have been added to the sample cell. The prominent NH_3 Q branch at 3336 cm^{-1} is clearly seen, even on single-shot exposures. To be seen clearly, the lines comprised by the P and R branches require averaging.

In Fig. 12, greatly averaged 27-kPa (200-torr) NH_3 spectra are photographed in second order. A relatively high degree of resolution is evidenced by the structure seen in the P and R branches. This again shows that the granular appearance of single-shot spectra does not have a systematic origin in the apparatus, as would be the case, for example, if Fabry-Perot etalons were inserted in the optical path. Figure 13 shows a densitometer trace of a similarly photographed NH_3 spectrum.

Methane at 40 kPa (300 torr) was photographed in first order in Fig. 14 and in second order in Fig. 15. The prominent CH_4 Q branch is at 3020 cm^{-1}. For both cases, the upconverted beam was amplified by cell C_4, containing a solution of bis-MSB in p-dioxane. Note that the amplifier tends to harshen the appearance of the random spectral noise.

Figures 16 and 17 contain second-order time-averaged spectra of two larger organic molecules, tetrahydropyran and quadricyclane. Remarkably strong Q branches are observed in both cases. Considerable destruction of quadricyclane was observed (Fig. 17) when $\approx$2.4 kPa (18 torr) of this gas, mixed with $\approx$2.0 kPa (15 torr) of SiF_4, was irradiated with about 50 laser pulses from a $\approx$0.5-J CO_2 TEA laser tuned to $\approx$1032 cm^{-1}. The CO_2 beam was unfocused as it was made to irradiate the gaseous sample in cell S.

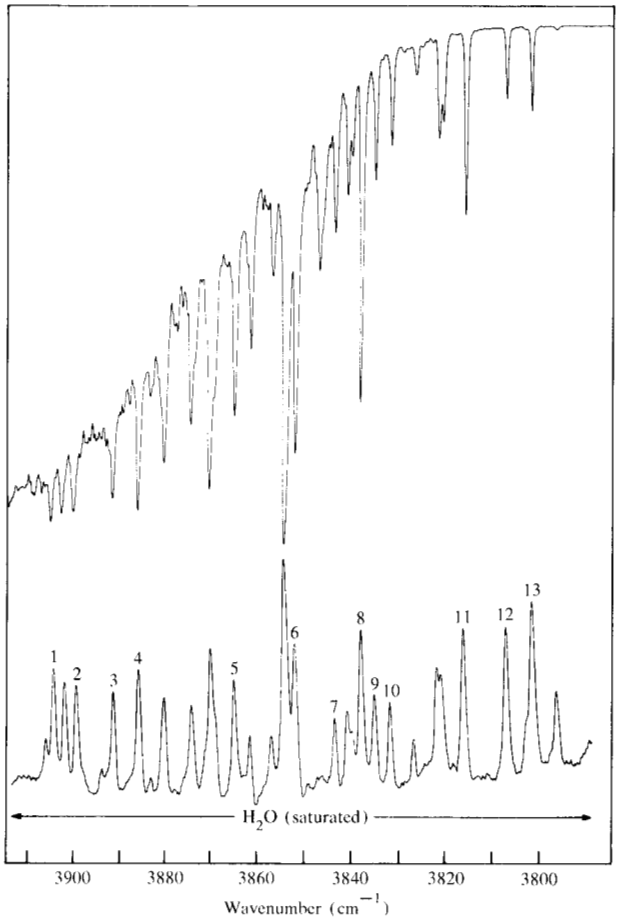

Figure 7 Comparison of densitometer trace of portion of spectrum shown in Fig. 6 (upper) with IUPAC calibration spectrum (lower).

• *Example of a transient spectrum: $CH_3NC \rightarrow CH_3CN$*

To demonstrate the *transient* capability of the new technique, the isomerization of methyl isocyanide to methyl cyanide was studied. This well-known isomerization is exothermic by 9.92×10^4 J/mole (23.7 kcal/mole) [8]. It has been suggested as an ideal unimolecular reaction for testing thermal explosion theories [9]. Recently we have observed that this thermal isomerization can be initiated by single pulses of CO_2 TEA laser radiation, tuned to coincide with the ν_4 band of the CH_3NC molecule [10].

The ν_1 band of CH_3NC, associated with the symmetric stretch of the CH_3 group, lies near 2966 cm^{-1} [11]. This range can be covered using the dye N,N′-bis(p-butoxybenzylidene)-α,α'-di-p-toluidine (BBOT) in ethanol in C_1 and C_2, and Stilbene 420 [in water + 3% NP10 surfactant (Exciton)] in the amplifier C_3. The top strip in Fig. 18 shows the upconverted spectrum of CH_3NC. In agreement with an earlier study by Thompson and Williams

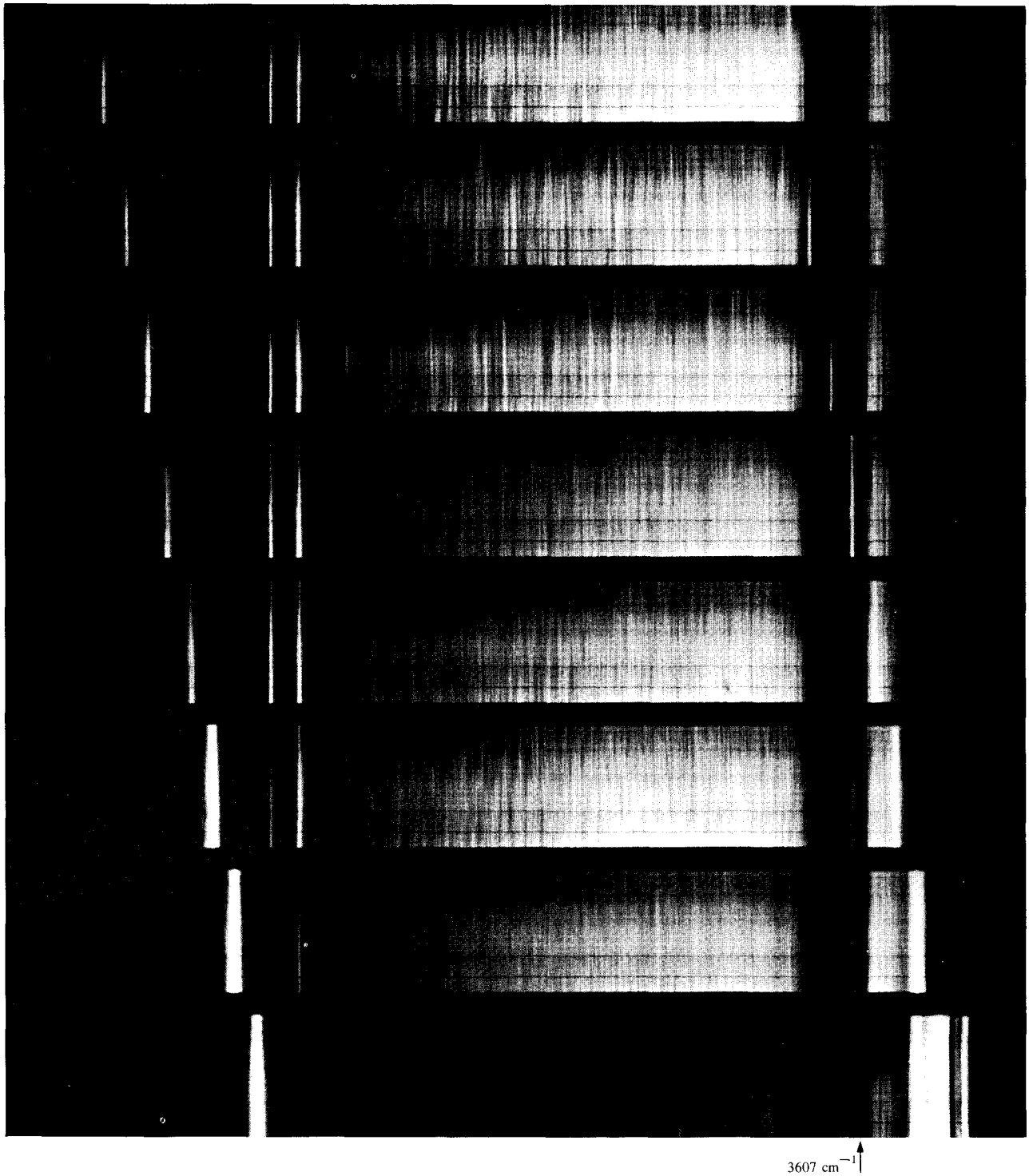

Figure 8 Series of spectra (first order) showing changes in appearance of upconverted light as the narrow band dye laser frequency ν_ℓ is stepped. Each spectrum represents four accumulated shots. The frequencies of the bright-line doublet at the left are 3165 and 3186 cm^{-1} (left to right).

[11], the P, Q, and R branch contours of the ν_1 band are clearly shown, but the P and R lines are not resolved. The sharp lines on the high-frequency side of the R branch of the ν_1 band belong to the ν_5 band. The isomerization product CH_3CN also has a ν_1 band centered at $\approx$2955 cm^{-1}, but the absorption band is too weak to be observed here.

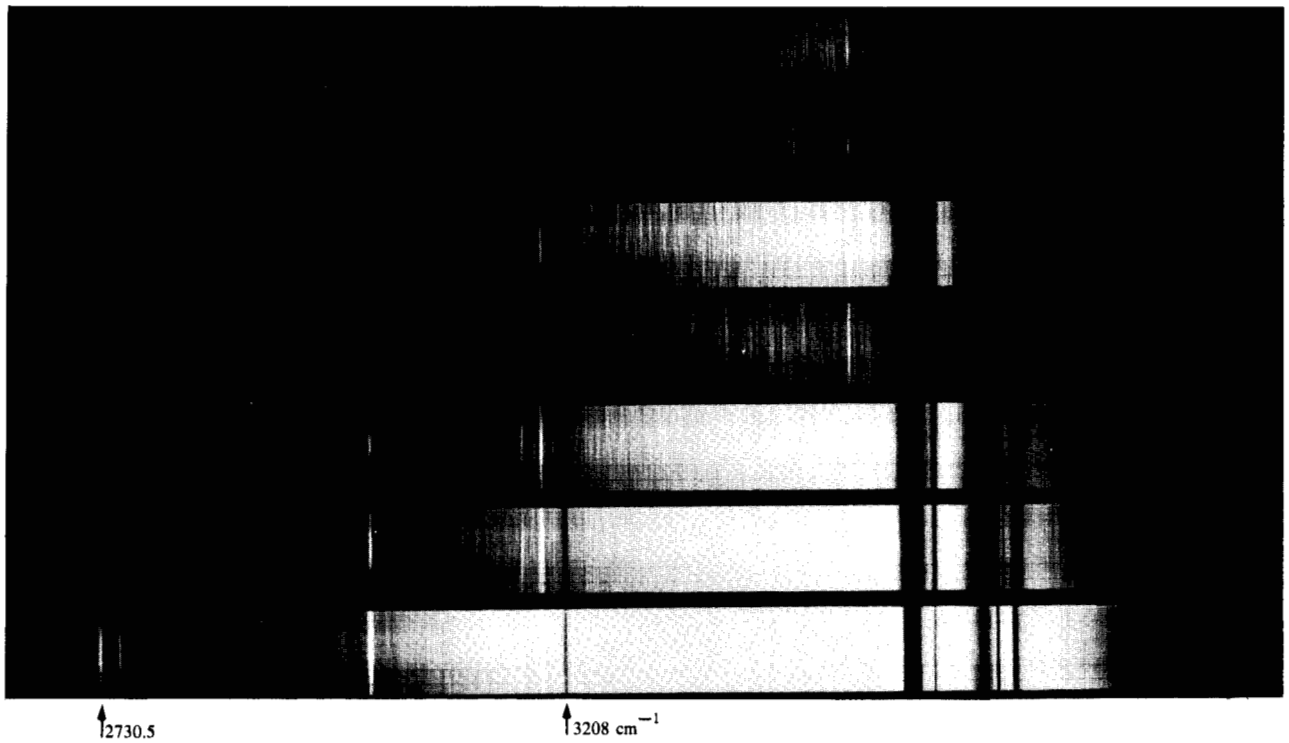

Figure 9 Series of spectra taken under the same basic conditions as in Fig. 8, except that ν_ℓ is fixed. The number of accumulated shots per exposure is 1, 1, 3, 2, 5, 10, and 20 (top to bottom). The 4s → 5p → 3d Stokes line is at ≈3000 cm^{-1}. The dark absorption band at 3208 cm^{-1} is due to absorption of the ir continuum by the 4d states of K in HP_2 (see text).

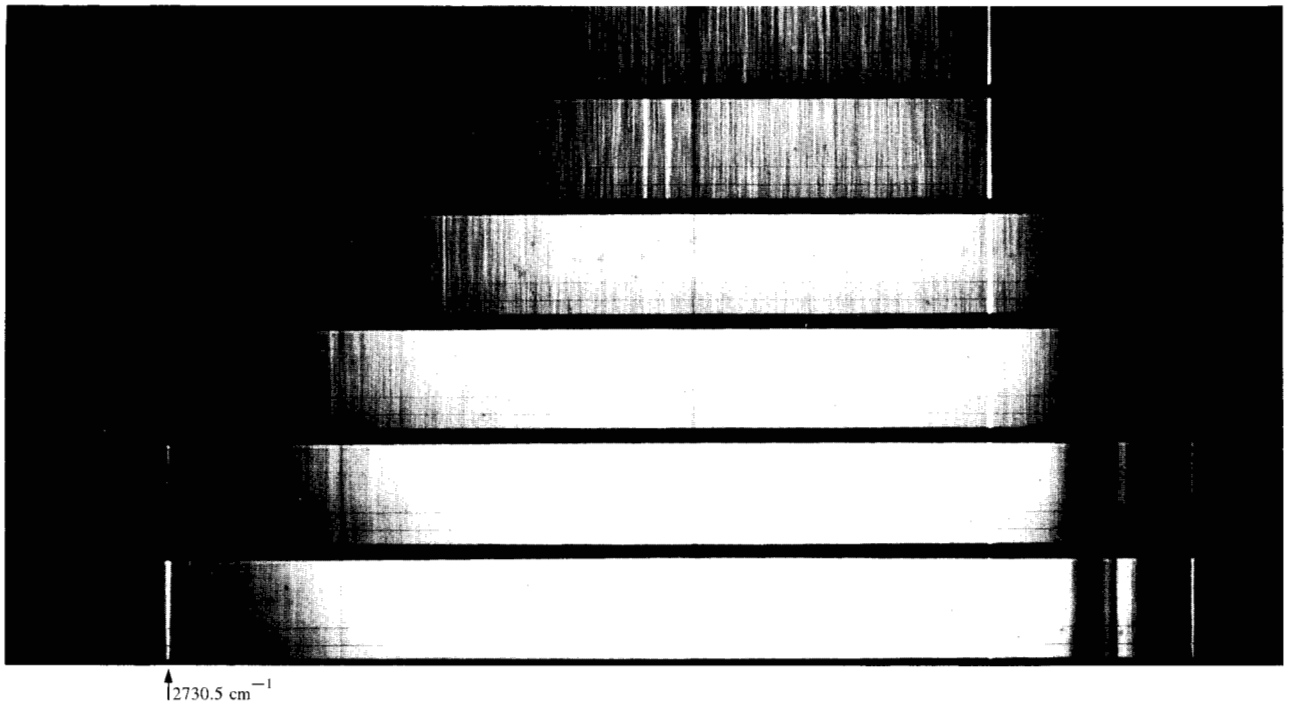

Figure 10 Upconverted dimethyl-POPOP Rb-K spectra with accumulated shots per exposure of 1, 3, 5, 7, 9, and 20 (top to bottom). No upconverted beam amplifier was used. The three lines at the left are at 2676.8, 2730.5, and 2749.2 cm^{-1}.

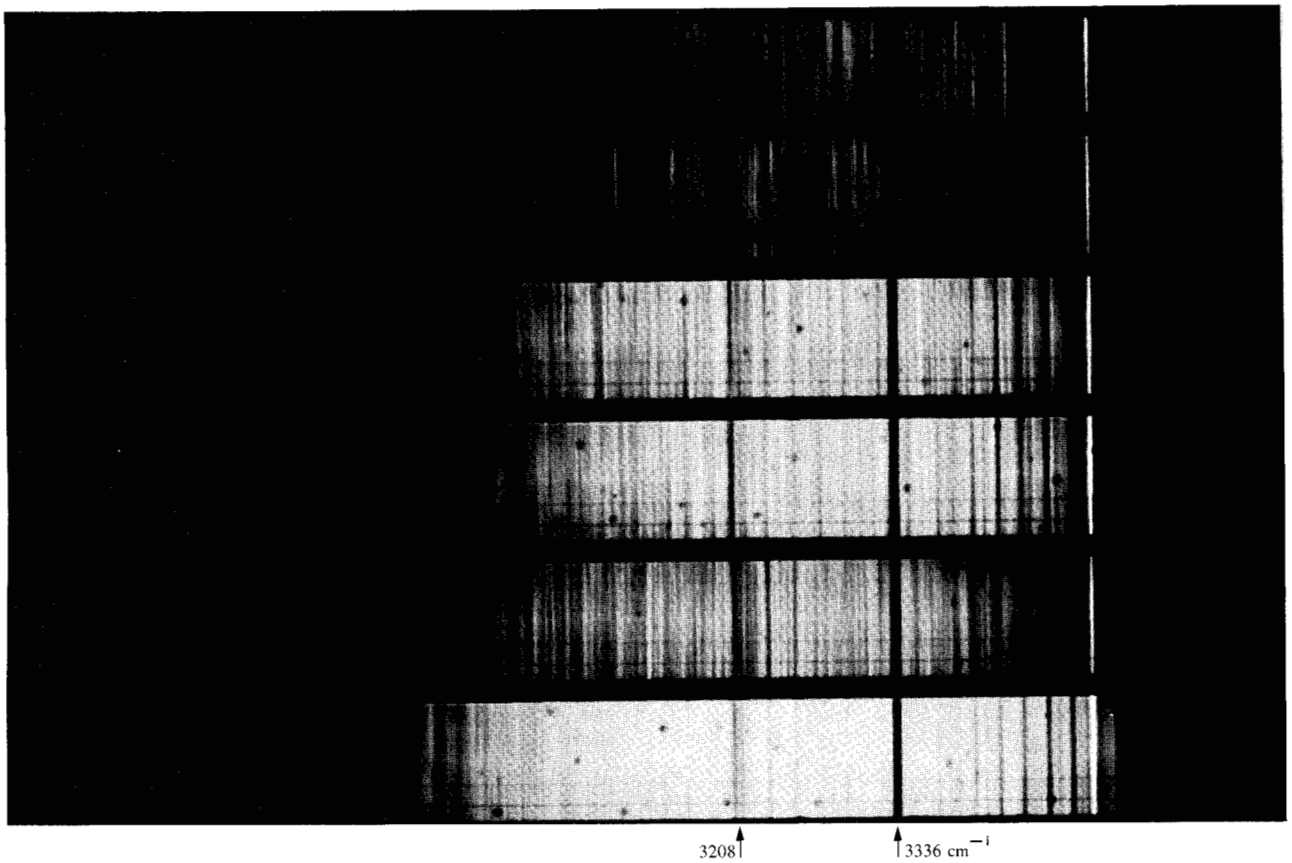

Figure 11 Dimethyl-POPOP Rb-K upconverted light spectra with ≈27 kPa (200 torr) NH_3 in the 18-cm sample (first order, upconverted beam not amplified). Accumulated shots per exposure are 1, 1, 3, 5, 3, and 10 (top to bottom). The NH_3 Q branch at 3336 cm^{-1} and the K 4d → 5f absorption at 3208 cm^{-1} are indicated.

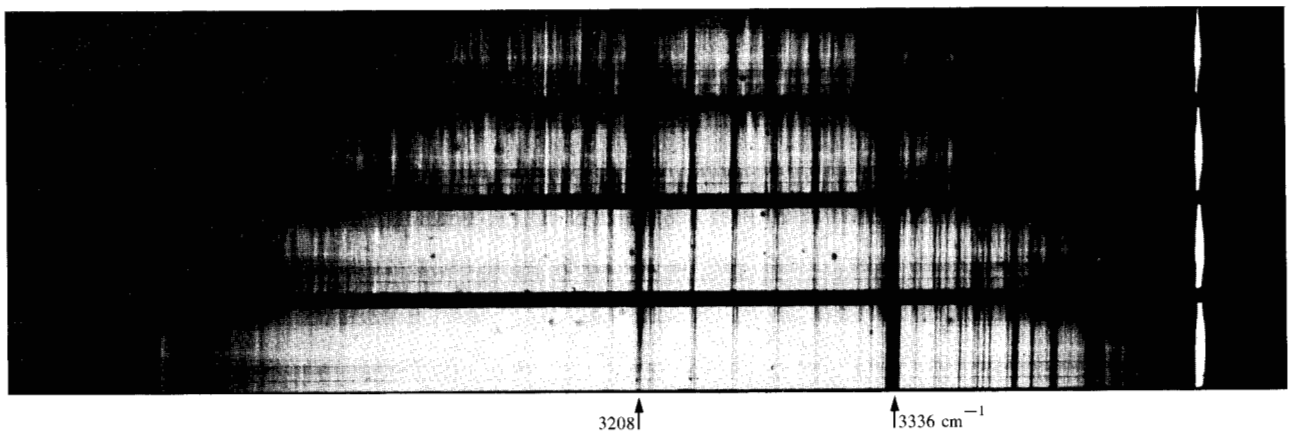

Figure 12 Dimethyl-POPOP Rb-K upconverted light spectra with ≈27 kPa (200 torr) NH_3 in sample cell (second order, upconverted beam not amplified). Shots per exposure are 25, 50, 100, and 200 (top to bottom).

Figure 18 shows the time-resolved upconverted spectra of CH_3NC [≈13 kPa (100 torr) initial pressure] taken at intervals of 1, 8, 17, 30, 100, and 265 μs, respectively, after the ≈0.5-J CO_2 laser pulse has initiated the thermal isomerization. Two effects can be clearly seen from these spectra. First, the intensity of the ν_1 absorption band

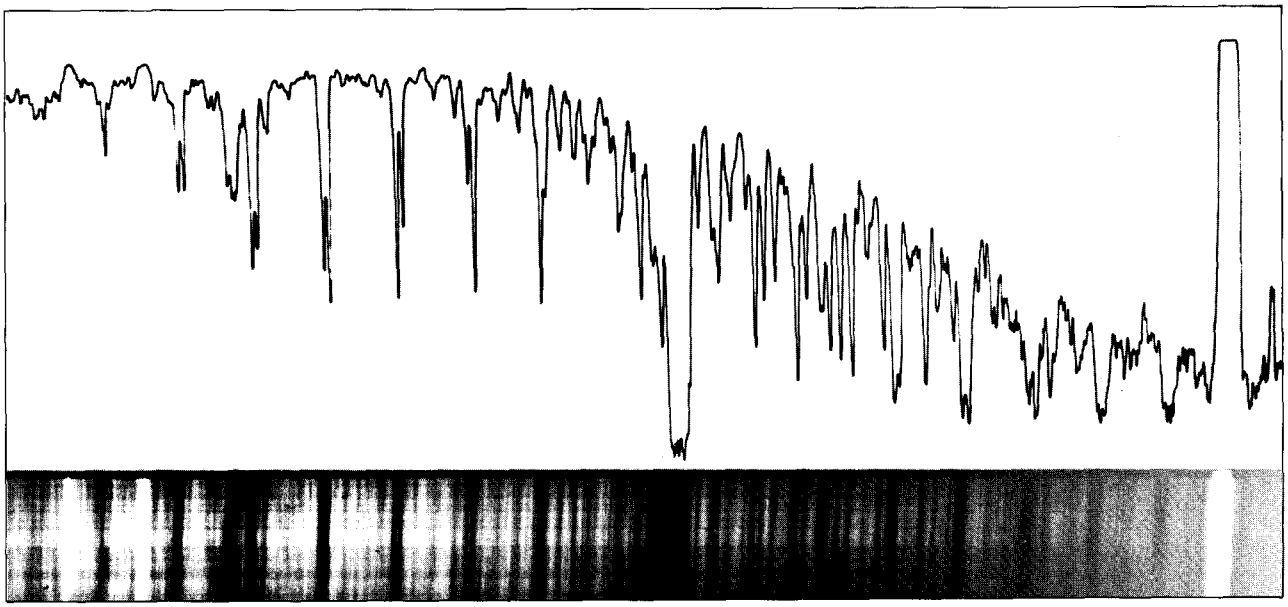

Figure 13 Densitometer trace of an NH_3 spectrum similar to that shown in Fig. 12.

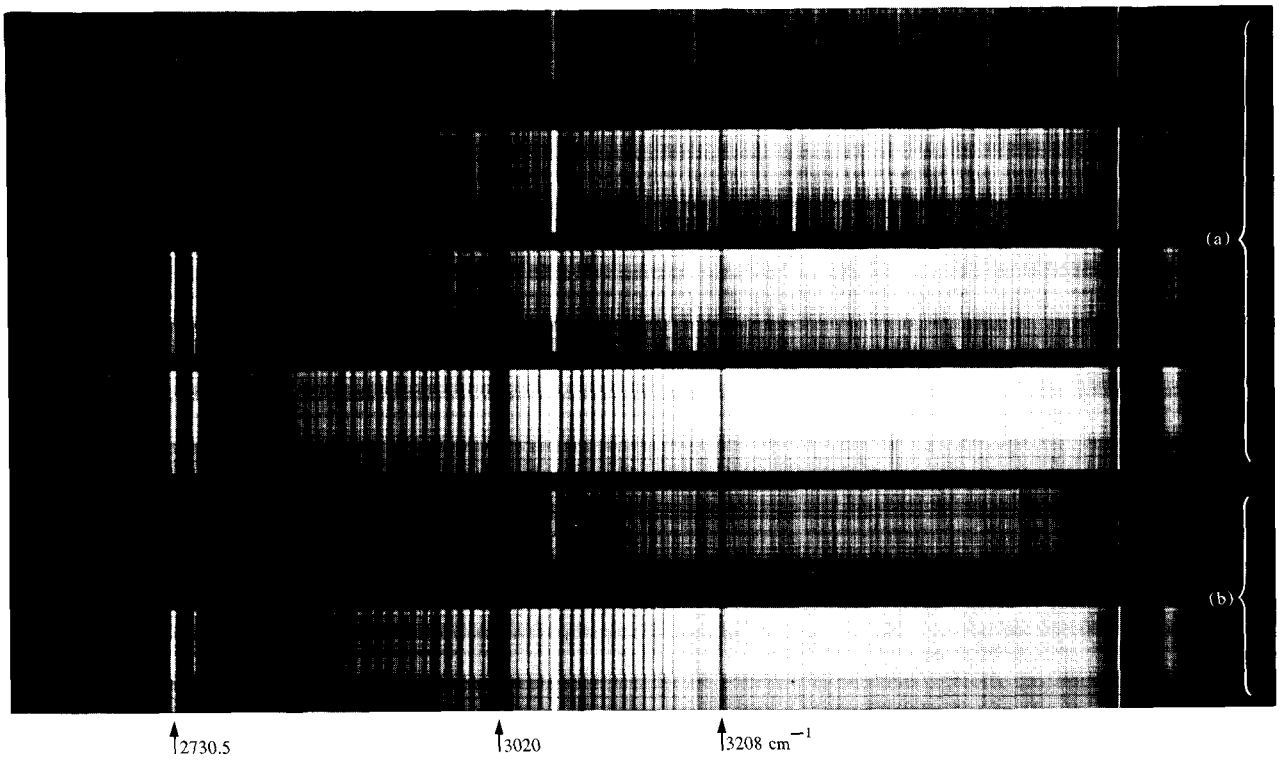

Figure 14 Methane spectra [first order, 40 kPa (300 torr)]; 10-μm slits. Cells C_1, C_2, and C_3 have 5×10^{-4} molar solutions of Stilbene 420 in 1:1 H_2O-CH_3OH. Amplifier cell C_4 is used with a solution of bis-MSB in p-dioxane. The prominent CH_4 Q branch at 3020 cm^{-1} is shown. Shots per exposure are (a) 1, 2, 3, and 5; and (b) 10 and 20 with a neutral density 1 filter on the spectrograph slit.

weakens as time increases. Second, the absorption band contours of the P and R branches broaden substantially, with maximum broadening occurring $\approx$30 μs after the laser pulse. This broadening is due to the increase in temperature from the energy released in the isomerization process. As shown by Gerhard and Dennison [12], for a

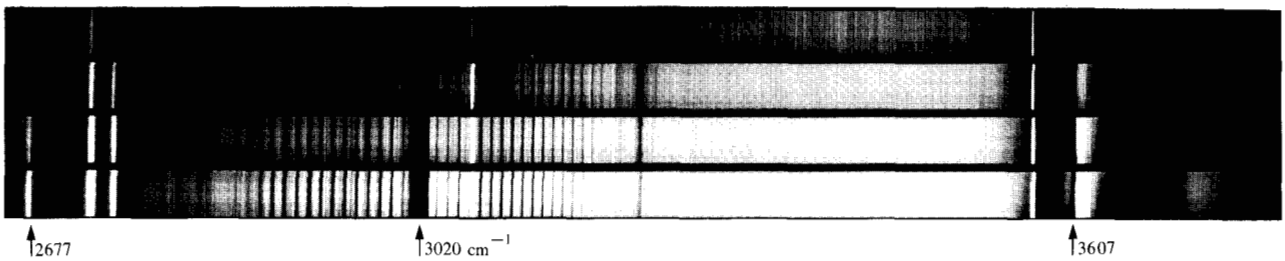

Figure 15 Methane spectra [second order, 40 kPa (300 torr)]; 50-μm slits. Same dyes as in Fig. 14. Shots per exposure are 10, 20, 30, and 50 (top to bottom).

Figure 16 Tetrahydropyran (THP) spectra (second order); 50, 100, and 150 (top to bottom) shots per exposure with sample cell (a) evacuated; (b) containing 0.4 kPa (3 torr) THP; and (c) containing 0.2 kPa (1.5 torr) THP.

parallel band transition in a symmetric rotator (*e.g.*, the ν_1 band of CH_3NC) the separation between the maxima of the P and R band contours is proportional to the square root of the absolute temperature. Using this relation and the measured separations between the P and R bands, we obtain the instantaneous temperature as a function of time; see Fig. 19. About 30 μs after the laser pulse, the temperature rises to about 673 K; it then gradually cools. (We note that this measured time behavior of the gas temperature was integrated over a volume that may have been larger than the effective interaction volume of the laser beam. Thus, the local temperature at the center of the latter may have risen substantially faster than indicated. To show the true rise in temperature determined by the isomerization rate, the reaction should be uniformly initiated with an unfocused CO_2 laser beam of cross section much larger than that of the probe beam. Unfortunately, this condition was not quite fulfilled in our experiment.) The maximum measured temperature of 673 K indicates this to be the approximate "threshold temperature" for thermal isomerization to CH_3CN; this is in reasonable agreement with thermal data [13]. Molecules of CH_3NC hotter than this threshold temperature rapidly isomerize to CH_3CN and are thus not detected by the ir probe. A true determination of the kinetic temperature could be made by seeding the CH_3NC gas with a small amount of stable foreign gas (such as methane) that has strong ir bands in a convenient range.

D. Theoretical considerations

In this section we give a theoretical description of the SERS process that generates the broad band infrared ra-

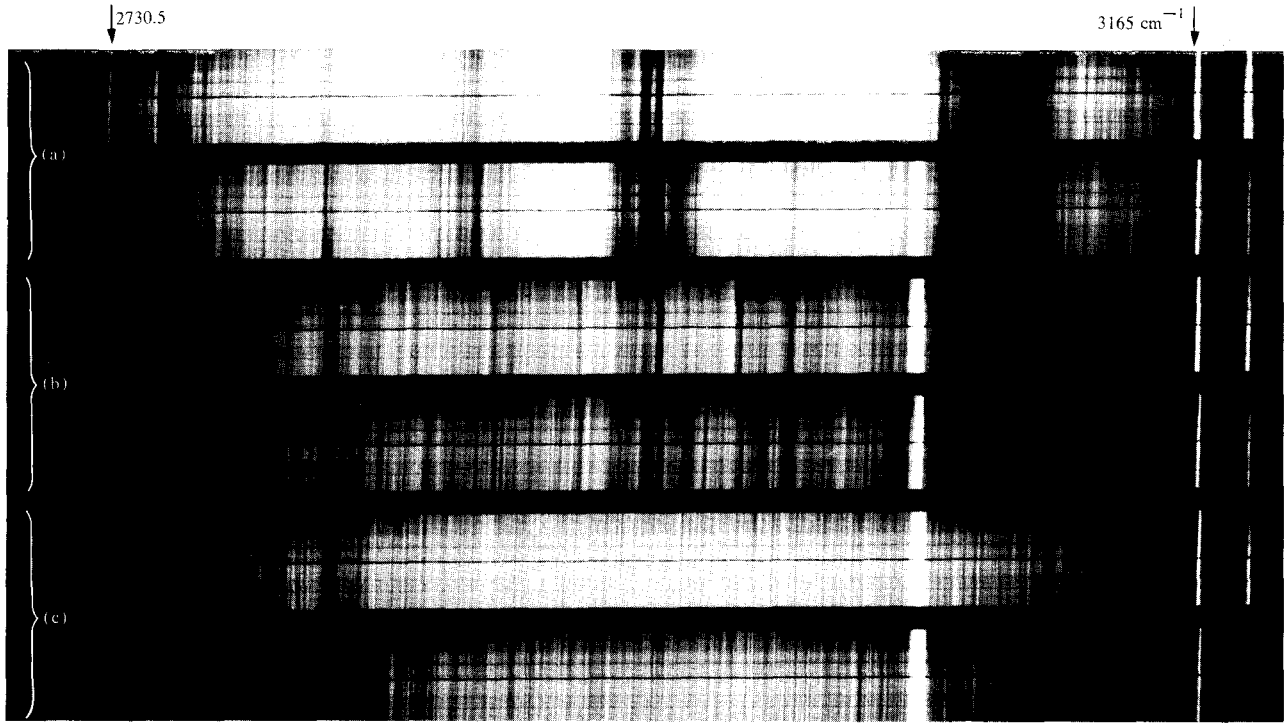

Figure 17 Quadricyclane spectra (second order); 16 and 24 shots per exposure (top, bottom) for sample cell containing (a) 2.4 kPa (18 torr) quadricyclane plus 2 kPa (15 torr) SiF_4; (b) as in (a), but sample gas previously irradiated with ≈50 pulses of CO_2 laser radiation ($\nu_{CO_2} \approx 1032$ cm^{-1}); and (c) as in (a), but sample cell evacuated. Cells C_1 and C_2 contain BBOT in ethanol; C_3, Stilbene 420 in H_2O plus 3% NP10; and C_4, POPOP in p-dioxane.

diation. It is of interest to try to explain why the infrared radiation has a smooth profile, even when the broad band pump overlaps the resonance lines of the metal vapor, and why the upconversion of the infrared occurs both smoothly and efficiently over a large spectral width, even in the presence of resonance lines and their accompanying dispersions.

Let us first discuss qualitatively the case of SERS with a broad band pump in the absence of linear or nonlinear dispersion. This problem has been studied both experimentally [14a, b] and theoretically [14b, 15] by many authors over the last decade. In this case, it is found that the threshold and gain of SERS are independent of pump bandwidth, and that the Stokes spectrum is virtually a replica of the pump spectrum, with the same spectral bandwidth.

These facts can be understood by considering the coupling between Stokes waves at different frequencies introduced by four-wave mixing processes of the form

$$P_{NL}(\omega_{S1}) = \chi^{(3)} E_P^*(\omega_{P2}) E_S(\omega_{S2}) E_P(\omega_{P1}),$$
$$P_{NL}(\omega_{S2}) = \chi^{(3)} E_P^*(\omega_{P1}) E_S(\omega_{S1}) E_P(\omega_{P2}), \quad (1)$$

where $E_P(\omega)$ is the Fourier transform of the pump pulse, P_{NL} is the nonlinear polarization, and subscripts S and P refer to the Stokes and pump quantities. In the absence of dispersion, the nonlinear susceptibiliy $\chi^{(3)}$ is a constant and the Stokes waves generated by these nonlinear polarizations are all phase matched.

In SERS the coupling leads to the cooperative growth of a Stokes wave with a spectrum related to the pump spectrum by

$$E_S(\omega_S) = C E_P(\omega_S + \Delta\omega_R), \quad (2)$$

where C is independent of the Stokes frequency ω_S and $\Delta\omega_R$ is the Raman shift frequency of the medium. Equation (2) implies that all pairs of pump and Stokes waves $\Delta\omega_R$ apart in frequency drive the Raman excitation with the same phase.

In the dispersive case two new elements enter that modify the simple result described above. First, linear dispersion introduces phase mismatch, which tends to destroy the coupling due to cooperative four-wave mixing of the various Stokes waves. Equally important is the dispersion in the Raman susceptibility $\chi^{(3)}$, which resonantly

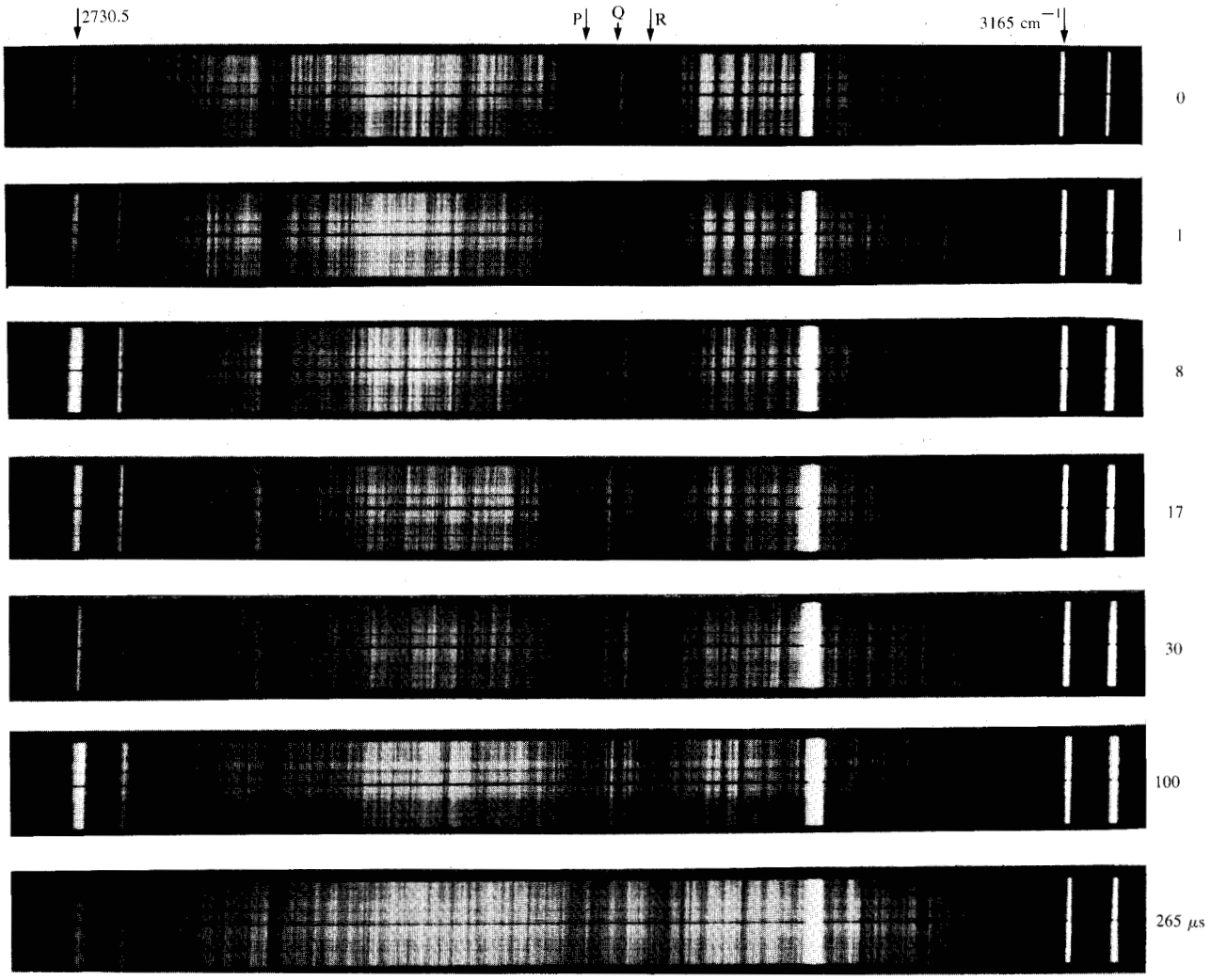

Figure 18 Changes in the upconverted spectra (second order) of ≈13 kPa (100 torr) CH_3NC as it thermally explodes (isomerizes), various times after the application of a ≈0.5-J pulse of CO_2 TEA laser radiation ($\nu \approx 960$ cm^{-1}). Each spectrum represents 16 superimposed shots; 50-μm slits; same dyes as in Fig. 17.

enhances the four-wave mixing processes. We show that these two competing effects compensate each other, resulting in a Raman *gain* that is remarkably flat, even for a broad band pump that overlaps resonance lines. In addition, the factor C in Eq. (2) must be frequency dependent and is peaked near the resonance lines, skewing the Stokes spectrum toward them.

Taking the equation for the Fourier transform of the slowly varying Stokes wave amplitude $E_S(z, \omega_S)$, we have, in the steady state case,

$$\frac{\partial E_S}{\partial z}(z, \omega_S) = -2\pi i \frac{\omega_S}{n_S c} P_{NL}(z, \omega_S) \exp[-ik(\omega_S)z], \qquad (3)$$

where n_S is the index of refraction $n(\omega_S)$, c is the speed of light, z is measured along the propagation direction, and $k(\omega_S) = n_S\omega_S/c$. The nonlinear polarization $P_{NL}(z, \omega_S)$ is given by

$$P_{NL} \exp[-ik(\omega_S)z] = \int \chi^{(3)}(-\omega_S, -\omega_P, \omega_S', \omega) \times [E_P^*(\omega_P)E_S(z, \omega_S')E_P(\omega) \exp(-i\Delta kz)]d\omega_P d\omega_S', \qquad (4)$$

where $\omega = \omega_P - \omega_S' + \omega_S$, $\Delta k = k(\omega_P) - k(\omega) + k(\omega_S) - k(\omega_S')$, and $E_P(\omega_P)$ is the Fourier transform of the pump electric field. The nonlinear susceptibility is

$$\chi^{(3)}(-\omega_S, -\omega_P, \omega_S', \omega) = \left(\frac{Ne^4}{\hbar^3}\right) \frac{|\langle ns|x|mp\rangle\langle mp|x|ms\rangle|^2}{(\omega_1 - \omega_P)(\Delta\omega_R - \omega_P + \omega_S' - i\gamma/2)(\omega_1 - \omega)} \equiv \chi_N^{(3)}[(\omega_1 - \omega_P)(\delta\omega - i\gamma/2)(\omega_1 - \omega)]^{-1}, \qquad (5)$$

where e is the electronic charge; ns and ms are the alkali ground and excited s states; $N = (N_{ns} - N_{ms})$ is the net

ground state number density; $\omega_1 = \omega_{mp,ns}$ (the resonance line frequency); $\Delta\omega_R = \omega_{ms,ns}$ (the electronic Raman shift); γ is the Raman linewidth (FWHM); and $\delta\omega = \Delta\omega_R - \omega_P + \omega_S'$ is the detuning of the pair ω_P, ω_S' from exact two-photon resonance. Combining Eqs. (3)-(5), we have

$$\frac{\partial E_S}{\partial z}(z, \omega_S) = -2\pi i \frac{\omega_S}{n_S c} \chi_N^{(3)} \times \int \frac{E_P^*(\omega_P) E_S(z, \omega_S') E_P(\omega) \exp(-i\Delta k z)}{(\omega_1 - \omega_P)(\delta\omega - i\gamma/2)(\omega_1 - \omega)} d\omega_P d\omega_S'. \quad (6)$$

As mentioned earlier, we expect the Stokes spectrum to be proportional to the pump spectrum. It will be convenient to define a function $f(z, \omega_S)$ by

$$E_S(z, \omega_S) = \left(\frac{\omega_S}{n_S}\right) \frac{E_P(\omega_S + \Delta\omega_R)}{(\omega_1 - \omega_S - \Delta\omega_R)} f(z, \omega_S). \quad (7)$$

Substituting into Eq. (6), we have

$$\frac{E_P(\omega_S + \Delta\omega_R)}{(\omega_1 - \omega_S - \Delta\omega_R)} \frac{\partial f}{\partial z}(z, \omega_S) = \frac{-2\pi i}{c} \chi_N^{(3)} \times \int \frac{E_P^*(\omega_P) E_P(\omega_P + \delta\omega) f(z, \omega_{PR} + \delta\omega) E_P(\omega_S + \Delta\omega_R - \delta\omega)}{(\omega_1 - \omega_P)(\delta\omega - i\gamma/2)(\omega_1 - \omega_P + \delta\omega)(\omega_1 - \omega_S + \delta\omega - \Delta\omega_R)} \times \exp(-i\Delta k z) d\omega_P d(\delta\omega), \quad (8)$$

where $\omega_{PR} = \omega_P - \Delta\omega_R$, and the integration variable ω_S' has been changed to $\delta\omega$.

At this point we must specify the properties of the pump light more completely. A temporally smooth pump intensity envelope with pulse width τ is assumed here. This determines the extent to which the pump wave amplitudes are correlated because of the exact relationship

$$\int E_P^*(\omega_P) E_P(\omega_P + \delta\omega) d\omega_P = \frac{1}{2\pi} \int |E(t)|^2 \exp(i\delta\omega t) dt, \quad (9)$$

where t is time and $E(t)$ is the Fourier transform of $E_P(\omega)$. The components are therefore correlated for $\delta\omega < \tau^{-1}$. In the steady state limit $\gamma >> \tau^{-1}$, we can thus make the approximation

$$E_P^*(\omega_P) E_P(\omega_P + \delta\omega) \approx \delta(\delta\omega) \frac{|E_P(\omega_P)|^2}{\tau} \approx \delta(\delta\omega) \frac{I(\omega_P)}{c}, \quad (10)$$

where $I(\omega_P)$ is the peak intensity per bandwidth. With this approximation, Eq. (8) reduces to

$$\frac{\partial f}{\partial z}(z, \omega_S) = \frac{4\pi\chi_N^{(3)}}{\gamma c^2} \int \frac{I(\omega_P) f(z, \omega_{PR}) \omega_{PR} \exp(-i\Delta k z)}{(\omega_1 - \omega_P)^2 n_{PR}} d\omega_P, \quad (11)$$

where n_{PR} is the refractive index corresponding to ω_{PR}. This is our basic equation describing the SERS process with linear and nonlinear dispersion included.

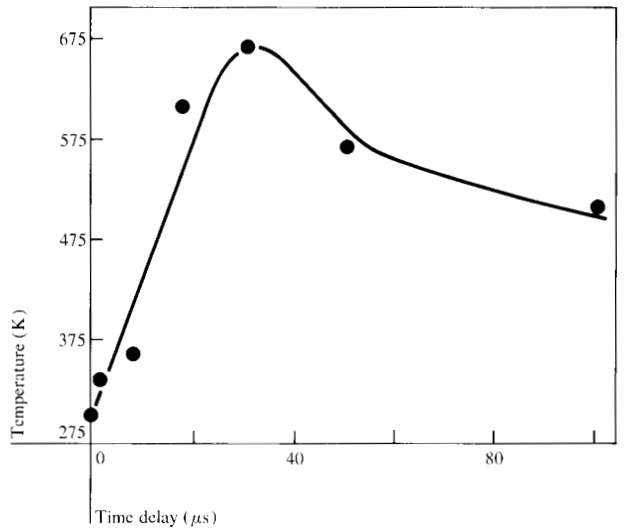

Figure 19 Temperature of the reacting CH_3NC gas as a function of time, determined from the separation of the P and R branches.

First, we consider the case where the pump band is tuned very far from resonance, so that $(\omega_1 - \omega_P)$ is much greater than the pump laser bandwidth $\Delta\omega_c$ (the subscript c refers to continuum). Then $\Delta k \approx 0$ and the factors multiplying $I(\omega_P)$ in the integral are nearly constant. The function f is then independent of frequency and grows exponentially with gain Γ,

$$\Gamma = \frac{4\pi\chi_N^{(3)}}{\gamma c^2} \left(\frac{\omega_S}{n_S}\right) \frac{I}{(\omega_1 - \omega_P)^2} = \frac{2\pi}{c^2} \chi^{(3)} \frac{\omega_S}{n_S} I, \quad (12)$$

where I is the peak pump intensity. In the broad band case, ω_S, n_S, and ω_P are interpreted as the values at the peaks of the Stokes and pump spectra. It is clear from Eq. (12) that the width of the pump has no effect on the gain, and that all Stokes frequency components grow with essentially the same gain. The overall Stokes spectrum in this case is given by

$$I_S(z, \omega_S) = C' \left(\frac{\omega_S}{n_S}\right)^2 \frac{I_P(\omega_S + \Delta\omega_R)}{(\omega_1 - \omega_S - \Delta\omega_R)^2} \exp(2\Gamma z), \quad (13)$$

where C' is independent of ω_S and can be estimated from the spontaneous Raman scattering cross section. The resonance denominator in the pre-factor is of the same form as one finds in the resonant Raman cross section.

While the nondispersive form of the broad band Raman scattering given by Eq. (13) works well even fairly near the resonance lines, a somewhat modified treatment is

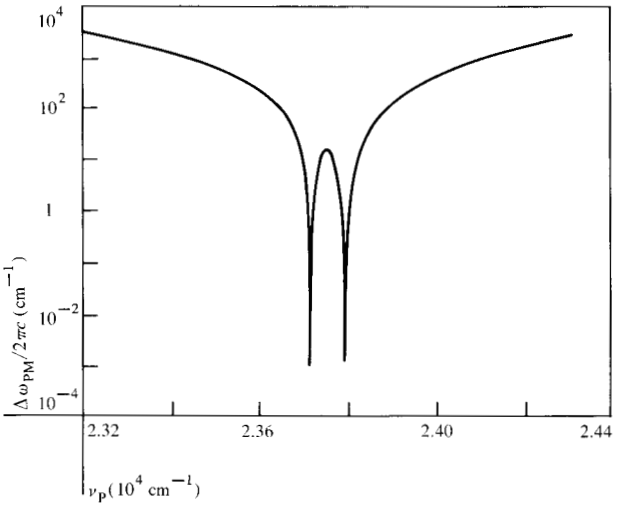

Figure 20 Phase-matching bandwidth $\Delta\omega_{PM}$ from Eq. (15) for Rb vapor; $N = 10^{17}/\text{cm}^3$, $z_0 = 1$ cm.

needed when we overlap the resonance lines. We begin by defining D, the derivative of the wave vector mismatch $\Delta k(\omega_P)$ with respect to ω_P:

$$D \equiv \frac{d\Delta k}{d\omega_P} \approx D_0/(\omega_1 - \omega_P)^2, \tag{14}$$

where $D_0 = \pi c r_0 N_{ns} f_{mp,ns}$, $r_0 = 2.818 \times 10^{-13}$ cm, and $f_{mp,ns}$ is the oscillator strength for the $ns \rightarrow mp$ transition. [Spin-orbit splitting modifies D in a simple way; see Eq. (19).]

If we define a characteristic length z_0, which describes the length over which the growth of the Stokes wave occurs, we can define an approximate *phase-matched bandwidth* $\Delta\omega_{PM}(\omega_P)$ by the relation

$$\Delta\omega_{PM} = \pi/z_0 D. \tag{15}$$

The length z_0 might be given by the vapor length, the beam confocal parameter, or the depletion length for the pump. The bandwidth $\Delta\omega_{PM}$ has the physical significance that the set of pump waves in a band of width $\approx\Delta\omega_{PM}$ all contribute to the growth of the Stokes wave at $(\omega_P - \Delta\omega_R)$ through phase-matched four-wave mixing processes. Furthermore, since a set of Stokes waves in a band of width $\Delta\omega_{PM}$ around a given wave (ω_S) are all coupled to one another and to a common set of pump waves, we do not expect the Raman gain to vary rapidly within a frequency span $\Delta\omega_{PM}$ around ω_S. With this in mind, we make the approximation that $f(z, \omega_{PR})$ in the integral in Eq. (11) can be replaced by its value at the center of the phase-matching band. Since $\Delta k = 0$ when $\omega_{PR} = \omega_S$, we replace $f(z, \omega_{PR})$ with $f(z, \omega_S)$ and remove it from the integral. With the additional approximations that (ω_{PR}/n_{PR}) varies slowly over a range $\Delta\omega_{PM}$, we also replace ω_{PR}/n_{PR} with ω_S/n_S, the value it has when $\Delta k = 0$. Finally, we observe that the resonance factor $R = (\omega_1 - \omega_P)^{-2}$ in the integral in Eq. (11) is essentially equal to D. Thus Eq. (11) becomes

$$\frac{\partial \ln f}{\partial z}(z, \omega_S) = \frac{4\pi\chi_N^{(3)}}{\gamma c^2}\left(\frac{\omega_S}{n_S}\right)\frac{1}{D_0} \times \int I(\omega_P)\exp(-i\Delta k z)d(\Delta k), \tag{16}$$

where ω_P is considered to be a function of Δk in the integral. We integrate with respect to $z(0 \rightarrow \infty)$ to get the total gain G_T. Since the exponential growth is due to the real part of the integral, we use

$$\text{Re}\int_0^\infty \exp(-i\Delta k z)dz = \pi\delta(\Delta k) \tag{17}$$

and find

$$G_T = \ln\left[\frac{f(\infty, \omega_S)}{f(0, \omega_S)}\right] = \frac{4\pi\chi_N^{(3)}}{\gamma c^2}\left(\frac{\omega_S}{n_S}\right)\frac{\pi}{D_0} I(\omega_S + \Delta\omega_R). \tag{18}$$

This gain depends on the spectral density rather than on the integrated intensity, and while it follows the pump profile, it shows no sharp peaks or dips at the resonance line position because of the balance between resonant enhancement and phase mismatching as we move over the resonance. This balancing persists even with a spin-orbit split doublet, in which case

$$R = \left[\frac{1}{3(\omega_{1/2} - \omega_P)} + \frac{2}{3(\omega_{3/2} - \omega_P)}\right]^2,$$

$$D = D_0\left[\frac{1}{3(\omega_{1/2} - \omega_P)^2} + \frac{2}{3(\omega_{3/2} - \omega_P)^2}\right], \tag{19}$$

where $\omega_{1/2} = \omega_{mp_{1/2},ns}$ and $\omega_{3/2} = \omega_{mp_{3/2},ns}$ so that $I(\omega_P)$ in the integral of Eq. (16) is multiplied by $F(\omega_P) = RD_0/D$, which can be put into the form

$$F(\omega_P) = \left[1 + \frac{2(\omega_{3/2} - \omega_{1/2})^2}{9(\omega_0 - \omega_P)^2}\right]^{-1}, \tag{20}$$

where $\omega_0 = (2\omega_{1/2} + \omega_{3/2})/3$. The notch function F has a null one-third of the way between $\omega_{1/2}$ and $\omega_{3/2}$, the frequencies corresponding to the resonance line doublet. The Stokes intensity spectrum in the highly dispersive "on resonance" case is given by

$$I_S(\infty, \omega_S) = C'\left(\frac{\omega_S}{n_S}\right)^2 \frac{I(\omega_S + \Delta\omega_R)}{(\omega_1 - \omega_S - \Delta\omega_R)^2}\exp(2G_T), \tag{21}$$

where G_T is taken from Eq. (18). [With spin-orbit splitting, the factor $(\omega_1 - \omega_S - \Delta\omega_R)^{-2}$ is replaced by R from Eq. (19), where now ω_P is replaced by $(\omega_S + \Delta\omega_R)$.]

Comparing the gains Γz [Eq. (12)] and G_T, we see that Γz increases as $(\omega_1 - \omega_P)^{-2}$ and depends on the total pump intensity I, whereas G_T is independent of $(\omega_1 - \omega_P)$ and

depends on the spectral density $I(\omega_P)$ for the very near or on resonance case. This exact behavior has recently been beautifully demonstrated by Korolev *et al.* [16] in Rb vapor, where a pump with bandwidth varied between 0.2 and 20 cm^{-1} drove SERS between the 5p and 6p states. In their experiment the measured threshold power varied along a parabola when the pump was tuned, except very near resonance, where the parabola was truncated and the threshold was constant. The threshold in the flat region increased with pump bandwidth, while it was independent of bandwidth in the parabolic regions away from the resonance line.

For our purpose we need a criterion for determining where the change from one regime to the other occurs. If $d(\Delta k)/d\omega_P$ is nearly constant over the pump bandwidth, the definition of $\Delta\omega_{PM}$ in Eq. (15) can be used. If $\Delta\omega_{PM} >> \Delta\omega_c$, the expressions for the nondispersive case can be used. If $\Delta\omega_{PM} << \Delta\omega_c$, we can use the "high dispersion" results of Eqs. (18) and (21). The function $\Delta\omega_{PM}(\omega_P)$ is plotted for Rb vapor where $N = 10^{17}$ atoms/cm^3 and $z_0 =$ 1 cm in Fig. 20.

For the more general case of a very broad pump overlapping resonance lines, the simple approximations using $d(\Delta k)/d\omega$ break down. As mentioned earlier, some physical feature must set a length scale z_0. The delta function in Δk then has a width of $\approx \pi/z_0$. Formally, we introduce into Eq. (16) a cut-off function $Z(z)$ to limit z to a length $\approx z_0$. For example, if a sharp cut-off at z_0 is used, we must replace the delta function in Eq. (17) with $\sin(\Delta k z_0)/\Delta k$, which leads to a total gain

$$G_T = \frac{4\pi\chi_N^{(3)}}{\gamma c^2}\int \frac{\omega_{PR} I(\omega_P)}{n_{PR}(\omega_1 - \omega_P)^2}\left(\frac{\sin \Delta k z_0}{\Delta k}\right) d\omega_P. \qquad (22)$$

For other forms of $Z(z)$, we replace $\sin \Delta k z_0/\Delta k$ in Eq. (22) with 2π Re $[Z(\Delta k)]$, where $Z(\Delta k)$ is the Fourier transform of $Z(z)$.

Figure 21(a) illustrates the type of experimental spectra obtained in the case where the pump slightly overlaps the Rb 5s-6p resonance lines. The upper curve is a densitometer trace of the spectrum of Stilbene 420 (7.5×10^{-4} molar in 2:1 H_2O-CH_3OH). The lower trace shows the *upconverted* spectrum obtained with the same Stilbene 420 continuum using the K upconverter. The strong skewing of the spectrum towards the resonance line is apparent. The absorption lines and nulls due to the Rb and K vapors are evident, and measurement shows the nulls are indeed quite accurately one-third of the way between the $p_{1/2}$ and $p_{3/2}$ components of the doublets.

For qualitative comparison, Fig. 21(b) shows a model pump spectrum (upper) and the corresponding *Stokes*

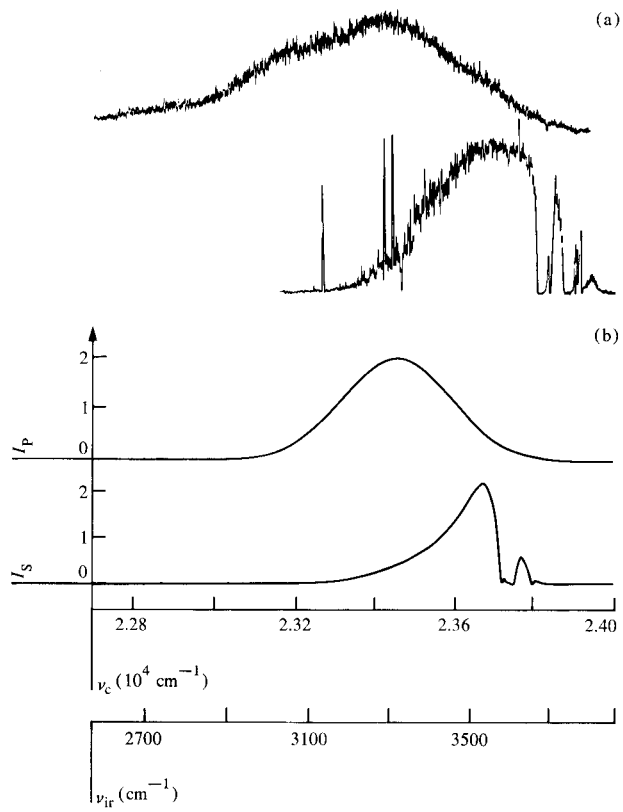

Figure 21 (a) Densitometer traces showing spectrum (single shot) of continuum beam ν_c (Stilbene 420, 2:1 H_2O-CH_3OH) photographed through Rb vapor (upper trace) and spectrum (ten shots) of corresponding upconverted beam (lower trace). (b) Model pump spectrum (upper trace) and corresponding calculated Stokes spectrum (lower trace).

spectrum calculated from Eq. (21), with G_T calculated from Eq. (22). In this case the cut-off function $Z(z) = \exp(-z/z_0)$ with $z_0 = 5$ mm was used. Thus, the $[\sin(\Delta k z_0)]/\Delta k$ function was replaced with a smoother Lorentzian, 2π Re $[Z(\Delta k)] = z_0/[1 + (\Delta k z_0)^2]$. Although no attempt was made to accurately model the spectra of Fig. 6(a), and no structure due to the upconversion process has been included, the overall shape of the Stokes spectrum in Fig. 21(b) does show considerable similarity to the upconverted spectrum of Fig. 21(a).

The combined four-wave mixing and SERS processes responsible for the upconversion in the second cell are still incompletely understood. In the usual parametric approximation, the narrow band SERS process establishes a coherent 4s-5s atomic superposition over some length of K vapor. The infrared then scatters from the oscillating atoms and generates both violet and orange sidebands of the atomic 4s-5s oscillation frequency at $\omega_{5s,4s} \pm \omega_{ir}$. For an s $\rightarrow$ s SERS process with the narrow band laser frequency ν_ℓ tuned outside the resonance line doublet, the

narrow band Stokes radiation at ν_S will have $\vec{E}_S$ parallel to $\vec{E}_\ell$. In this case the upconversion of the infrared is described by

$$\frac{\partial \vec{E}_u}{\partial z} = -2\pi i \frac{\omega_u}{n_u c} \vec{P}_{NL}(z, \omega_u) \exp[-ik(\omega_u)z], \tag{23}$$

$$\vec{P}_{NL}(z, \omega_u) \exp[-ik(\omega_u)z] = \left[\frac{Ne^2}{\hbar} \sum_{m'} \frac{\langle ns|x|m'p\rangle\langle m'p|x|ms\rangle}{(\omega_{m'p} - \omega_u)}\right] \times \vec{E}_{ir}\rho(z) \exp(i\Delta kz), \tag{24}$$

where $k(\omega_u) = n_u\omega_u/c$ and $\rho(z)$ is the spatially slowly varying (ms, ns) off-diagonal density matrix element describing the Raman excitation driven by the SERS process, $\omega_u = \omega_{5s,4s} + \omega_{ir}$, and $\Delta k = k(\omega_\ell) - k(\omega_S) + k(\omega_{ir}) - k(\omega_u)$. For spin-orbit split doublets, $(\omega_{m'p} - \omega_u)^{-1}$ is replaced by $[1/3(\omega_{m'p_{1/2}} - \omega_u)^{-1} + 2/3(\omega_{m'p_{3/2}} - \omega_u)^{-1}]$. Integration of Eq. (23) with respect to z leads to an upconverted intensity spectrum,

$$I_u(\omega_u) = \left(\frac{2\pi\omega_u}{n_u c}\right)^2 \left[\frac{Ne^2}{\hbar} \sum_{m'} \frac{\langle ns|x|m'p\rangle\langle m'p|x|ms\rangle}{(\omega_{m'p} - \omega_u)}\right]^2 \times I_{ir}(\omega_{ir})[2\pi\rho(\Delta k)]^2, \tag{25}$$

where $\rho(\Delta k)$ is the Fourier transform of $\rho(z)$. There are two main features of interest in Eq. (25): the resonant enhancement near the K resonance lines and the factor $[\rho(\Delta k)]^2$, which governs the bandwidth limitation of the upconversion imposed by phase matching. The very striking broad band nature of the upconversion process, together with its high efficiency, is evidence that phase matching is not important. One possible explanation for this is that the SERS process has very high gain (several hundred cm^{-1}). This may give a short "active region," where $\rho(z)$ is largest and the Stokes wave grows rapidly while the pump intensity falls. If this region were only a few millimeters long, $\rho(\Delta k)$ would be correspondingly broad and fairly large wave vector mismatching could be tolerated.

E. Conclusion

We have tried to illustrate the characteristics of this new ir technique with the spectra presented in this paper. The advantages of the technique lie in its ability to record instantaneously information contained in a broad spectral range. The isomerization of methyl isocyanide indicates, in our opinion, the type of reaction to which this technique may best be applied. Dynamic changes occurring in various media can be detected, provided the latter are not too rarified; *e.g.*, the technique would seem to be readily applicable to the field of combustion engineering. Another straightforward application is in the study of laser-induced pyrolysis of polymers. We have, in fact, recently obtained time-resolved spectra showing changes in the $\approx$3000-cm^{-1} bands of a polyvinyl film upon pyrolysis with a CO_2 TEA laser pulse. The technique would also be clearly suitable for studying the development of gain in chemical laser systems. For example, hydrogen fluoride elimination reactions [17] could be studied in this way. The possible presence of two-photon gain in infrared systems could also be monitored conveniently with our technique.

The main disadvantage of the technique stems from the presence of random spectral noise in the upconverted spectra. Ten to twenty shots per exposure are required for decent averaging of the spectral noise, *i.e.*, for the true linear features of the sample absorption spectrum to become apparent. This noise is also seen in the spectrum of the orange continuum beam $\nu_c - 2\nu_{ir}$. There is evidence [Fig. 21(a)] that the noise originates in the visible/uv continuum beam and is then accentuated by the Raman process occurring in HP_1.

One question, discussed in the introduction, concerns other ranges of ir that can be probed in the same manner as the 2600- to 4000-cm^{-1} region. In this connection, two specific suggestions for alternate broad band Raman sources can be made. One is to use high-pressure molecular hydrogen as the Raman scattering medium. With intense broad band continuum beams produced by red and near-infrared dyes, one might be able to reach the $\approx$5-μm region via two consecutive Stokes shifts, followed by four-wave mixing to generate an ir continuum, effectively at the third Stokes frequency. The upconverter cell could still be an alkali metal vapor. One advantage of this scheme is that it uses the stronger second harmonic of the ND^{3+}:YAG laser system.

Another way to extend the ir range that still retains use of the well-engineered Nd^{3+}:YAG laser is a two-step Raman pumping scheme [16]. One could simultaneously irradiate an alkali metal Raman cell with two laser beams. One beam would populate the lowest-lying p states, *e.g.*, 3p in the case of Na. The other beam, an intense visible continuum beam, would then generate broad band SERS in a sequence such as 3p $\rightarrow$ nd $\rightarrow$ np in Na. This would produce broad band ir radiation centered at frequencies well removed from the ir ranges listed in Table 1. In Na with n = 5, 6, the generated ir would be at $\approx$5 μm, 10 μm, respectively. A variant of this scheme would be based upon broad band stimulated electronic *hyper*-Raman scattering, represented by a sequence such as 3s $\rightarrow$ 3p $\rightarrow$ nd $\rightarrow$ np in Na.

Acknowledgments

This work is partially supported by the U.S. Army Research Office (Contract No. DAAG 29-76-C-0062) and the

Office of Naval Research (Contract No. N00014-76-C-0907). We would like to thank our colleague J. Ors for preparation of the CH_3NC sample. D. S. Bethune thanks both R. L. Byer, Applied Physics Dept., Stanford University, CA, and J. L. Carlsten, Los Alamos Laboratory, NM, for providing preprints of their work on stimulated broad band Raman scattering.

References

1. Y. Talmi, *Appl. Opt.* **17,** 2489 (1978).
2. T. R. Gurski, H. W. Epps, and S. P. Maran, *Appl. Opt.* **17,** 1238 (1978).
3. A. W. Mantz, *Appl. Opt.* **17,** 1347 (1978); Hajime Sakai and Randall E. Murphy, *Appl. Opt.* **17,** 1342 (1978).
4. D. S. Bethune, J. R. Lankard, and P. P. Sorokin, *Opt. Lett.* **4,** 103 (1979).
5. See for example J. J. Wynne and P. P. Sorokin, in *Nonlinear Infrared Generation*, Y.-R. Shen, Ed., Springer-Verlag, New York, 1977, Ch. 5.
6. D. Cotter, D. C. Hanna, and R. Wyatt, *Opt. Commun.* **16,** 256 (1976).
7. *Tables of Wavenumbers for the Calibration of Infrared Spectrometers*, International Union of Pure and Applied Chemistry (IUPAC) Commission on Molecular Structure and Spectroscopy, Pergamon Press, New York, 1977, p. 98.
8. M. H. Baghal-Vayjooee, J. L. Collister, and H. O. Pritchard, *Can. J. Chem.* **55,** 2634 (1977).
9. H. O. Pritchard and B. J. Tyler, *Can. J. Chem.* **51,** 4001 (1973).
10. D. S. Bethune, J. R. Lankard, M. M. T. Loy, J. Ors, and P. P. Sorokin, *Chem. Phys. Lett.* **57,** 479 (1978).
11. H. W. Thompson and R. L. Williams, *Trans. Faraday Soc.* **48,** 502 (1952).
12. S. L. Gerhard and D. M. Dennison, *Phys. Rev.* **43,** 197 (1933).
13. F. W. Schneider and B. S. Rabinovitch, *J. Amer. Chem. Soc.* **84,** 4215 (1962).
14. (a) V. V. Bocharov, A. Z. Grasyuk, I. G. Zubarev, and V. F. Mulikov, *Sov. Phys. JETP* **29,** 235 (1969); A. Z. Grasyuk, I. G. Zubarev, and N. V. Suyazov, *JETP Lett.* **16,** 166 (1972). See also G. P. Dzhotyan, Yu. E. D'yakov, I. G. Zubarev, A. B. Mironov, and S. I. Mikhailov, *Sov. J. Quantum Electron.* **7,** 783 (1977) and references therein.
(b) W. R. Trutna, Y. K. Park, and R. L. Byer, *IEEE J. Quantum Electron.* (in press) and references therein.
15. Yu. E. D'yakov, *JETP Lett.* **11,** 243 (1970); R. L. Carman, F. Shimizu, C. S. Wang, and N. Bloembergen, *Phys. Rev. A* **2,** 60 (1970); S. A. Akhmanov, Yu. E. D'yakov, and L. I. Pavlov, *Sov. Phys. JETP* **39,** 249 (1974). See also M. G. Raymer, J. Mostowski, and J. L. Carlsten, *Phys. Rev. A* (in press) and references therein.
16. F. A. Korolev, V. A. Mikhailov, and V. I. Odintsov, *Opt. Spectroscopy* **44,** 535 (1978).
17. T. D. Padrick and G. C. Pimentel, *J. Phys. Chem.* **76,** 3125 (1972).

Received March 21, 1979; revised April 26, 1979

The authors are located at the IBM Thomas J. Watson Research Center, Yorktown Heights, New York 10598.